Transition Mechanism from Brittle Fracture to Ductile Shear when Machining Brittle Materials with an Abrasive Waterjet

Chuanzhen Huang[1,#], Hongtao Zhu[1], Xinyu Lu[1], Quanlai Li[1] and Cuilian Che[1]

1 Center for Advanced Jet Engineering Technologies (CaJET), School of Mechanical Engineering, Shandong University, Jinan, 250061, China
Corresponding Author / E-mail: chuanzhenh@sdu.edu.cn, TEL:+86-531-88396913, FAX: +86-531-88396913

KEYWORDS: Abrasive waterjet machining, Machining mechanism, Brittle materials

Critical erosion kinetic energy models for radial/median cracks and lateral cracks in a workpiece are established in this study. We used experimental results to demonstrate that the fracture erosion resistance and erosion machining number could be used to evaluate the brittle fracture resistance and machinability of a workpiece. Erosion kinetic energy models were developed to predict brittle fracture and ductile shear, and a critical erosion kinetic energy model was developed to predict the transition from brittle fracture to ductile shear. These models were verified experimentally.

Manuscript received: October 25, 2007 / Accepted: December 21, 2007

NOMENCLATURE

A = chip shape factor for the target material
C_v = orifice efficiency
C_y = compressibility coefficient
C_η = general erosion kinetic energy efficiency
$C_{\delta V}$ = fracture factor about the crack mode
$C_{\delta V}^L$ = fracture factor for lateral cracks
$C_{\delta V}^R$ = fracture factor for radial/median cracks
H = hardness of the target material
M = fracture erosion machinable number ($J^{-1/6}$)
m_p = abrasive particle mass (kg)
P_w = water pressure (MPa)
R' = ratio of abrasive/water mass flow rates
R_{ce} = fracture erosion resistance (J)
U_{Kin} = erosion kinetic energy absorbed by the target material (J)
U_{KinC} = crack critical erosion kinetic energy (J)
U_{KinC}^L = critical erosion kinetic energy for lateral cracks (J)
U_{KinC}^R = critical erosion kinetic energy for radial/median cracks (J)
v_p = abrasive particle speed (m/s)
α' = shape factor of the indenter
β = dimensionless target material constant
δV = crack indentation volume (m^3)
δV_C^L = fracture critical indentation volume for lateral cracks (m^3)
δV_C^R = fracture critical indentation volume for radial/median cracks (m^3)
η = momentum transfer efficiency
η_{ero} = erosion kinetic energy efficiency
μ = dimensionless constant
ρ_w = water density (kg/m^3)

1. Introduction

The recent use of brittle materials such as glass and ceramics for a variety of high-performance applications has increased the need for developing a high-precision material removal method.[1-3] The concept of ductile mode machining has led to many innovative applications for machining brittle materials, such as single point diamond turning[4,5] and ductile-regime grinding.[5,7] When ductile mode machining of brittle materials is achieved, flawless machining free of brittle fractures is obtained. Abrasive waterjet machining is a powerful tool for processing various materials,[8] especially brittle materials such as glass and ceramics. Abrasive waterjet machining is generally understood to be a rapid erosion process, and determining the erosion mechanisms is key to understanding this process.[9]

Numerous studies on the erosion caused by solid particles impacting on brittle materials indicate two types of erosion modes: brittle and ductile.[10] For brittle materials, a greater erosion rate can be obtained under a brittle erosion mode while a finely eroded

surface can be obtained under a ductile erosion mode. Brittle and ductile modes of erosion can occur in the same brittle material, and the transition between them can be controlled by changing the erosion conditions.[11] Therefore, brittle or ductile erosion can be controlled by changing abrasive waterjet machining conditions to obtain a greater efficiency or higher surface quality. However, a systemic investigation on brittle–ductile transition in abrasive waterjet machining has not yet been performed.

In this report, a theoretical analysis is used to examine the erosion of brittle materials in abrasive waterjet machining based on the indentation theory for hard angular particles. Brittle and ductile erosion models are discussed and a brittle–ductile transition critical erosion kinetic energy model is derived. Experimental verification is then used to establish the applicability of the brittle–ductile transition critical erosion kinetic energy model.

2. Indentation Fracture Analysis on the Erosion Mechanisms of an Abrasive Waterjet

2.1 Erosion Mechanisms for a Single Abrasive Particle

The erosion of brittle materials by a single hard angular abrasive particle is known as indentation fracture.[12,13] This type of fracture is characterized by plastic deformation of the contact area between the impacting particle and the target, with subsurface lateral cracks propagating outward from the base of the contact zone on planes nearly parallel to the surface and radial cracks propagating from the contact zone normal to the surface. The lateral cracks are responsible for material removal while the radial cracks are the source of strength degradation. Figure 1 shows a simplified diagram of such an event, but in reality more than one lateral and redial/median crack can be present.

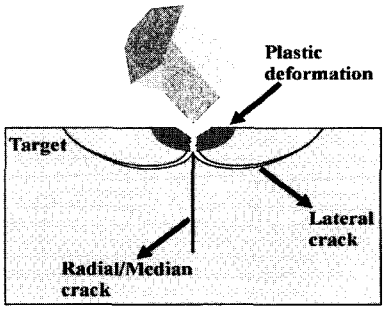

Fig. 1 Simplified schematic drawing of crack formation by a single hard angular abrasive particle impact[14]

Slikkerveer *et al.* established the fracture threshold crack indention volume.[15] For radial/median cracks,

$$\delta V_C^R = \left(\frac{3}{2\pi}\right)^3 \frac{\mu^6}{\beta^6} \frac{E^{3/2} K_{IC}^6}{H^{15/2}} \tag{1}$$

and for lateral cracks,

$$\delta V_C^L = \frac{1}{3} \frac{\zeta_0^{3/2}}{\alpha'^{1/2} A^3} \frac{E^{3/2} K_{IC}^6}{H^{15/2}} . \tag{2}$$

Using the energy consideration principle, the erosion kinetic energy absorbed by the target material is equal to the work done during the impact. Therefore, the indentation volume δV equals the ratio between the erosion kinetic energy absorbed by the target material and the hardness of the target material,

$$\delta V = \frac{U_{Kin}}{H} . \tag{3}$$

Equations (1) and (2) can be rewritten as a critical erosion kinetic energy equation. For radial/median cracks,

$$U_{KinC}^R = \left(\frac{3}{2\pi}\right)^3 \frac{\mu^6}{\beta^6} \frac{E^{3/2} K_{IC}^6}{H^{13/2}} \tag{4}$$

and for lateral cracks,

$$U_{KinC}^L = \frac{1}{3} \frac{\zeta_0^{3/2}}{\alpha'^{1/2} A^3} \frac{E^{3/2} K_{IC}^6}{H^{13/2}} . \tag{5}$$

Equations (4) and (5) can be rewritten as a universal equation,

$$U_{KinC} = C_{\delta V} \frac{E^{3/2} K_{IC}^6}{H^{13/2}} , \tag{6}$$

where the value of the constant $C_{\delta V}$ depends on the type of crack. For radial/median cracks,

$$C_{\delta V}^R = \left(\frac{3}{2\pi}\right)^3 \frac{\mu^6}{\beta^6} \tag{7}$$

and for lateral cracks,

$$C_{\delta V}^L = \frac{1}{3} \frac{\zeta_0^{3/2}}{\alpha'^{1/2} A^3} . \tag{8}$$

The term $E^{3/2} K_{IC}^6/H^{13/2}$ consists of three material property parameters and has the same dimensions as energy. It is an energy term that denotes the erosion kinetic energy absorbed by the target material before fracture, representing the capability of the target material to resist fracture. The term can be defined as a "fracture erosion resistance," R_{CE}, expressed as

$$R_{CE} = \frac{E^{3/2} K_{IC}^6}{H^{13/2}} . \tag{9}$$

Another material constant can be defined as a "fracture erosion machinable number," M, expressed as

$$M = (R_{CE})^{-1/6} = \left(\frac{E^{3/2} K_{IC}^6}{H^{13/2}}\right)^{-1/6} . \tag{10}$$

2.2 Evaluation of the Fracture Erosion Resistance and Fracture Erosion Machinable Number

A group of erosion experiments was performed to evaluate R_{CE} and M. Three types of material, silicate glass, 96% alumina, and silicon nitride, were tested, and garnet abrasives with 100 and 120 grit, a Mohs hardness of 8, and a density of 4.0 g/cm^3 were used. The main mechanical properties, R_{CE}, and M of the three materials are listed in Table 1. The values for R_{CE} and M were calculated using Eqs. 9 and 10, respectively. The erosion rates of the three materials under various waterjet pressures were measured. The experimental results are shown in Fig. 2.

The silicate glass had the smallest R_{CE} and the highest M. Silicate glass also had the highest erosion rate for all waterjet pressures. Silicon nitride had the highest R_{CE} and the smallest M, and had the smallest erosion rates for all waterjet pressures. These results indicated that a smaller R_{CE} and larger M leads to more prominent fracture erosion and higher erosion rates. Therefore, R_{CE} and M can be used to directly evaluate the erosion resistance and machinability of materials.

Table 1 Main mechanical properties, R_{CE}, and M of the target materials

Material	E [GPa]	H [GPa]	K_{IC} [MPam$^{1/2}$]	R_{ce} [J×10^{-12}]	M [J$^{-1/6}$]
Silicate glass	69	5.6	0.8	2.0587	88.6614

96% Al_2O_3	300	18	4	147.49	43.5049
Si_3N_4	311	16	8	14556	20.2214

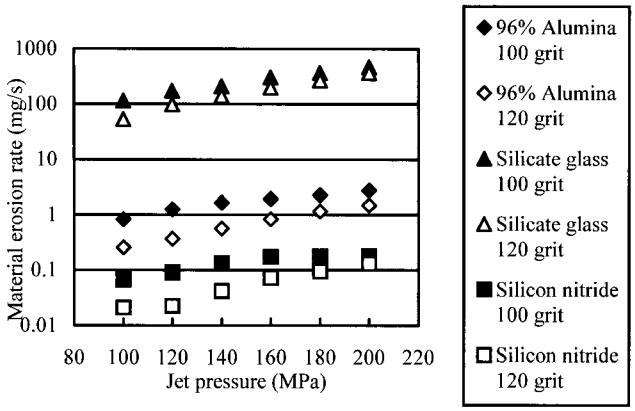

Fig. 2 Material erosion rates of three types of brittle material versus jet pressure of the abrasive waterjet

3. Transition Mechanism from Brittle Fracture to Ductile Shear

3.1 Erosion Kinetic Energy of a Single Abrasive Particle

In abrasive waterjet systems, abrasive particles are sucked into the waterjet from a hopper to the mixing chamber. An abrasive particle is accelerated by the waterjet within a short mixing tube and obtains its erosion kinetic energy before arriving at the target material. According to the research by Hashish[16], the abrasive particle velocity in an abrasive waterjet can be calculated by

$$v_p = \frac{\eta C_v C_y}{1+R'}\sqrt{\frac{2P_w}{\rho_w}}. \tag{11}$$

Considering the energy loss in an erosion process, the erosion kinetic energy of an abrasive particle absorbed by the target material is given by

$$U_{KinP} = \eta_{ero}\frac{1}{2}m_p v_p^2. \tag{12}$$

Using Eqs. (11) and (12), the erosion kinetic energy of the abrasive particle can be rewritten as

$$U_{kinP} = C_\eta\left(\frac{\rho_p}{\rho_w}\right)\left(\frac{1}{1+R'}\right)^2 d_p^3 P_w, \tag{13}$$

where the constant C_η is

$$C_\eta = \frac{\pi}{6}\eta_{ero}\eta^2 C_v^2 C_y^2. \tag{14}$$

3.2 Transition Mechanism

If the erosion kinetic energy of an abrasive particle absorbed by the target material exceeds the critical brittle fracture erosion kinetic energy, material is removed by fracturing; otherwise, material is removed by a flow-type ductile shear erosion mechanism. Therefore, the critical erosion kinetic energy for transition from brittle fracture erosion to ductile shear erosion can be obtained from

$$U_{kinP} = U_{KinC}. \tag{15}$$

This can be rewritten as

$$\left(\frac{\rho_p}{\rho_w}\right)\left(\frac{1}{1+R'}\right)^2 d_p^3 P_w = \frac{C_{\delta V}^{(R)(L)}}{C_\eta}\frac{E^{3/2}K_{IC}^6}{H^{13/2}}. \tag{16}$$

If

$$\left(\frac{\rho_p}{\rho_w}\right)\left(\frac{1}{1+R'}\right)^2 d_p^3 P_w \geq \frac{C_{\delta V}^{L}}{C_\eta}\frac{E^{3/2}K_{IC}^6}{H^{13/2}}, \tag{17}$$

then lateral cracks occur, and material is removed as the cracks propagate. If

$$\frac{C_{\delta V}^{L}}{C_\eta}\frac{E^{3/2}K_{IC}^6}{H^{13/2}} > \left(\frac{\rho_p}{\rho_w}\right)\left(\frac{1}{1+R'}\right)^2 d_p^3 P_w \geq \frac{C_{\delta V}^{R}}{C_\eta}\frac{E^{3/2}K_{IC}^6}{H^{13/2}}, \tag{18}$$

then lateral cracks do not occur, and material is removed by a ductile shear mechanism. In this case, radial/median cracks do occur. If

$$\left(\frac{\rho_p}{\rho_w}\right)\left(\frac{1}{1+R'}\right)^2 d_p^3 P_w < \frac{C_{\delta V}^{R}}{C_\eta}\frac{E^{3/2}K_{IC}^6}{H^{13/2}}, \tag{19}$$

then material is removed by the ductile shear mechanism without any fracturing.

Figure 3 illustrates the brittle–ductile transition critical erosion kinetic energy model based on the erosion of 96% alumina ceramic by alumina abrasive particles. The constants $C_{\delta V}^R$ and $C_{\delta V}^L$ were calculated using $\mu = 0.63$,[15] $\beta = 0.096$,[17] $\zeta_0 = 1.2\times10^3$,[18] $\alpha' = 2$,[19,20] and $A = 0.75$.[18] Therefore, $C_{\delta V}^R \approx 8.6944\times10^3$ and $C_{\delta V}^L \approx 2.3225\times10^4$. In Fig. 3, energy level I (3.4255×10^{-6} J) is the critical erosion kinetic energy for lateral crack propagation and energy level II (1.2823×10^{-6} J) is the critical erosion kinetic energy for radial/median crack propagation.

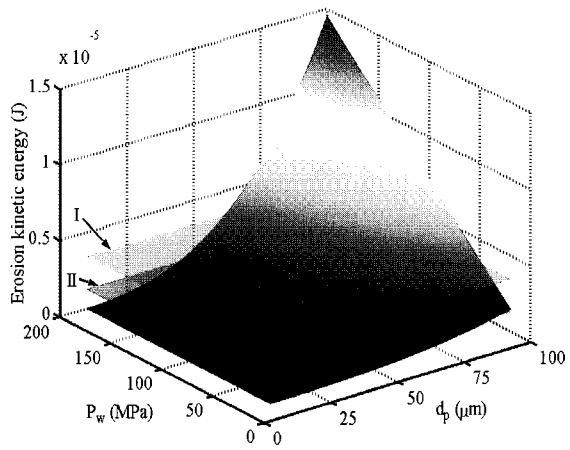

Fig. 3 Brittle–ductile transition critical erosion kinetic energy model

3.3 Experimental Verification of the Transition Mechanism

3.3.1 Experimental Procedure

Material erosion rates and erosion surface morphologies after applying the abrasive waterjet under different erosion kinetic energy levels were studied to analyze the transition of the erosion mechanism. Silicate glass and 96% alumina ceramic were used as the target materials. Their mechanical properties are listed in Table 2. All erosion experiments were performed with alumina abrasive, which had the mechanical properties listed in Table 3. Five groups of experiments were conducted with a FCM 1313 waterjet cutter, which used a jewel orifice with a diameter of 0.254 mm and a carbide nozzle with a diameter of 0.762 mm and a length of 75 mm. The experimental conditions are listed in Table 4. The erosion rates were measured with a JA2103 electronic balance with a precision of 1 mg. The eroded surfaces of the workpieces were observed under a scanning electron microscope (SEM).

Table 2 Mechanical properties of the target materials

Material	E [GPa]	Hv [Gpa]	K_{IC} [Mpam$^{1/2}$]	ρ [g/cm^3]
Silicate glass	69	5.6	0.8	2.5
96% Al_2O_3	300	18	4	3.7

Table 3 Mechanical properties of the abrasive

Abrasive	Composition [%]			Hv [GPa]	ρ [g/cm^3]
	Al_2O	SiO_2	Fe_2O_3		
Al_2O_3	≥99 %	<0.3 %	<0.15%	20	3.95

Table 4 Experimental conditions

Erosion condition	Target material	Abrasive particle	Average diameter [μm]	Jet pressure [MPa]	Stand-off distance [mm]	Erosion angle [°]	Traverse speed [mm/min]
1	Silicate glass	Al_2O_3	150,120 109,75 38,18	120	15	60	100
2	96% Al_2O_3	Al_2O_3	150,120 109,75 38,18	120	5	60	50
3	Silicate glass	Al_2O_3	120	120	15	90,75 60,45 30,15	100
4	96% Al_2O_3	Al_2O_3	120	120	5	90,75 60,45 30,15	50
5	Silicate glass	Al_2O_3	120	100,120 140,160 180,200	15	60	100
6	96% Al_2O_3	Al_2O_3	120	100,120 140,160 180,200	5	60	50

3.3.2 Results and Discussion

Figure 4 shows the relationship between the material erosion rate and the erosion kinetic energy of the abrasive particles for silicate glass and 96% Al_2O_3. Under the same erosion kinetic energy, the material erosion rate was dependent on the mechanical properties of the target material, while for a given material, the material erosion rate was mainly dependent on the erosion kinetic energy of the abrasive particles. The material erosion rates of the silicate glass were higher than that of the 96% Al_2O_3 ceramic.

The change in the material erosion rate with the erosion kinetic energy was similar between the two materials. Three energy regions were observed: a low erosion kinetic energy region, a high erosion kinetic energy region, and a transition region. In the low erosion kinetic energy region, the material erosion rate increased slowly with the erosion kinetic energy. In the high erosion kinetic energy region, the material erosion rate increased quickly with the erosion kinetic energy, indicating a different dominant erosion mechanism in different erosion kinetic energy regions. In theory, the transition between the two mechanisms is located at the point where the two regions meet, but in fact, a region of transition connects the two different erosion mechanisms.

Further analysis on the transition of erosion mechanisms can be performed using the relationship between the erosion specific energy and the erosion kinetic energy of the abrasive particles, as shown in Fig. 5. In the low erosion kinetic energy region, the erosion specific energy is very high; the opposite is true in the high erosion kinetic energy region. This indicates that the erosion in the low erosion kinetic energy region consumed more energy while the erosion in the high erosion kinetic energy region was more efficient. This analysis also indicates that a transition region connected the two different erosion mechanisms.

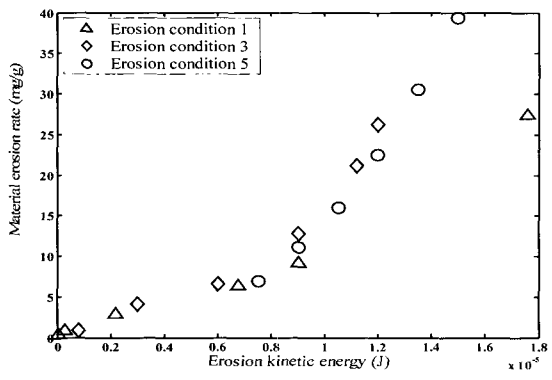

(a) Silicate glass

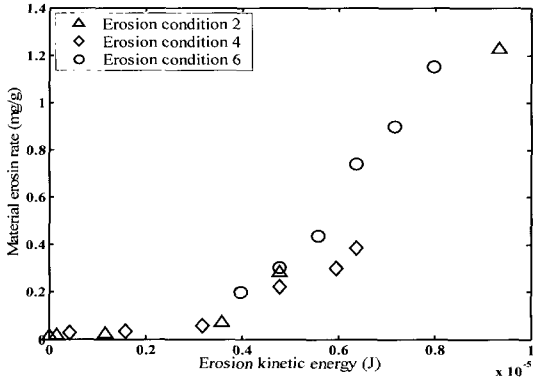

(b) 96% Al_2O_3 ceramic

Fig. 4 Material erosion rate versus abrasive particle kinetic energy

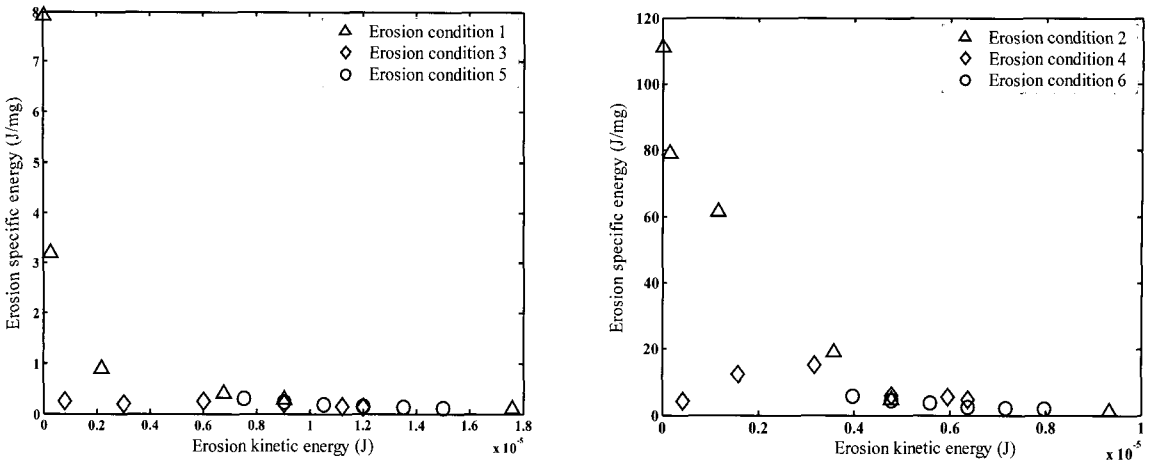

(a) Silicate glass (b) 96%Al_2O_3 ceramic

Fig. 5 Erosion specific energy rate versus abrasive particle kinetic energy

An analysis of the eroded surfaces was used to confirm the erosion mechanism for different erosion kinetic energies. Figures 6 and 7 show SEM pictures of the erosion surfaces in low, high, and transition erosion kinetic energy regions.

The erosion surfaces in the high erosion kinetic energy region (Figs. 6(a) and 7(a)) were entirely composed of fracture surfaces. For silicate glass, this type of fracture was characterized by cracks propagating outward from the base of the contact zone on the site impacted by the abrasive particles, nearly parallel to the surface of the workpiece. Some cracks propagating normal to the workpiece surface from the impacting site were also visible. For 96% Al_2O_3 ceramic, the fracturing was mainly caused by intergranular cracks, which indicates that the erosion mechanism of the low erosion kinetic energy region was brittle fracture erosion.

The erosion surfaces in the high erosion kinetic energy region (Figs. 6(b) and 7(b)) were mainly composed of plastic surfaces and several small cracks or flaws. During the erosion process, the target material did not fracture and the eroded surface quality was very fine. The material was removed mainly by ductile shear and micro cuts, indicating that the erosion mechanism of the high erosion kinetic energy region was ductile shear erosion.

The erosion surfaces in the transition erosion kinetic energy region (Figs. 6(c) and 7(c)) were composed of both fracture surfaces and plastic surfaces. Cracks and grooves caused by micro cuts were clearly visible. This shows that both brittle erosion and ductile erosion were dominant erosion mechanisms. The erosion mechanism can be defined as partial ductile shear erosion.

The microstructure of the target material had a prominent effect on the erosion process. Glass can be thought of as a type of homogeneous elastic–plastic material. Obvious flaws are not observed in silicate glass specimens. Therefore, the erosion process in silicate glass can be modeled very well using indentation fracture mechanics. However, some flaws occur in alumina ceramics, such as crystal boundaries and pores. The microstructure flaws of the target material can affect the nucleation and propagation of cracks caused by impacting abrasive particles, making the brittle–ductile transition region of alumina ceramic wider than that of silicate glass.

These results demonstrate that a brittle–ductile erosion transition region does exist when machining brittle material using an abrasive waterjet. In brittle fracture erosion, the material erosion rate is high and the specific energy is small; therefore, the machining efficiency is high. In ductile shear erosion, the material erosion rate is low and the specific energy is high; therefore, the machining efficiency is low but the eroded surface is fine. In the transition region, the machining efficiency and erosion surface.quality fall between those of brittle and ductile erosion.

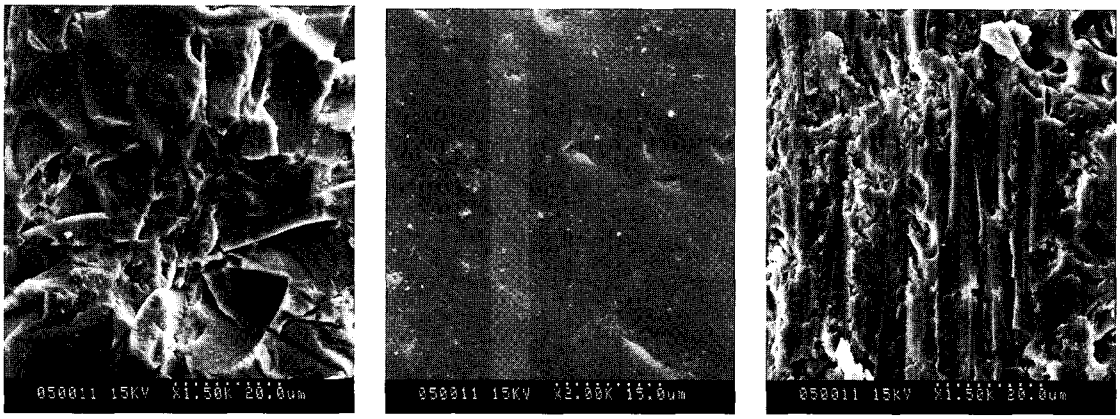

(a) Brittle fracture erosion (b) Ductile shear erosion (c) Partial ductile shear erosion

$U_{kinP} = 1.76 \times 10^{-5} J$ $U_{kinP} = 3.04 \times 10^{-8} J$ $U_{kinP} = 2.86 \times 10^{-7} J$

Fig. 6 Silicate glass eroded surface

(a) Brittle fracture erosion $U_{kinP} = 9.34 \times 10^{-6} J$

(b) Ductile shear erosion $U_{kinP} = 1.61 \times 10^{-8} J$

(c) Partial ductile shear erosion $U_{kinP} = 1.52 \times 10^{-7} J$

Fig. 7 96% Al_2O_3 ceramic eroded surface

4. Conclusions

We established critical erosion kinetic energy models for radial/median cracks and lateral cracks in a workpiece using an indentation fracture analysis on the erosion mechanisms of an abrasive waterjet. We applied the concepts of fracture erosion resistance and erosion machining number directly to evaluate the erosion resistance and machinability of materials.

We investigated the transition mechanism from brittle fracture erosion to ductile shear erosion theoretically and experimentally and established critical erosion kinetic energy models for the transition from brittle fracture to ductile shear. Experimental results verified that a brittle–ductile transition region does exist when machining brittle material using an abrasive waterjet. During brittle fracture erosion, the material erosion rate was high and the specific energy was small; therefore, the machining efficiency was high. A finely eroded surface was obtained after ductile shear erosion. In the transition region, the machining efficiency and erosion surface quality fell between those of brittle fracture erosion and ductile shear erosion.

The microstructures of the target material had a prominent effect on the erosion process. Material flaws, such as crystal boundaries and pores, affected the nucleation and propagation of cracks caused by impacting abrasive particles.

Ductile shear erosion from abrasive waterjets can be used to achieve micro-material removal, leaving a finely eroded surface with little damage. This is a promising precision machining method for brittle materials.

ACKNOWLEDGMENT

This study was supported by the Key Project of the Shandong Natural Science Foundation (Z2005F02), China.

REFERENCES

1. Isobe, H., Hara, K., Kyusojin, A., Okada, M. and Yoshihara, H., "Ultrasonically Assisted Grinding for Mirror Surface Finishing of Dies with Electroplated Diamond Tools," International Journal of Precision Engineering and Manufacturing, Vol. 8, No. 2, pp. 38-43, 2007.
2. Kim, H. T., Yang, H. J. and Kim, S. C., "Control Method for the Tool Path in Aspherical Surface Grinding and Polishing," International Journal of Precision Engineering and Manufacturing, Vol. 7, No. 4, pp. 51-56, 2006.
3. Lee, S. K., Miyamoto, Y., Kuriyagawa, T. and Syoji, K., "Minimization of Hydrodynamic Pressure Effect on the Ultraprecision Mirror Grinding," International Journal of Precision Engineering and Manufacturing, Vol. 6, No. 1, pp. 59-64, 2005.
4. Blackley, W. S. and Scattergood, R. O., "Ductile-Regime Machining Model for Diamond Turning of Brittle Materials," Precision Engineering, Vol. 13, No. 2, pp. 95-103, 1991.
5. Blake, P. N. and Scattergood, R. O., "Ductile-Regime Machining of Germanium and Silicon," Journal of the American Ceramic Society, Vol. 73, No. 4, pp. 949-957, 1990.
6. Bifano, T. G, Dow, T. A. and Scattergood, R. O., "Ductile-Regime Grinding: A New Technology for Machining Brittle Materials," Journal of Engineering for Industry, Vol. 113, Issue 2, pp. 184-189, 1991.
7. Zhong, Z. W., "Ductile or Partial Ductile Mode Machining of Brittle Materials," International Journal of Advanced Manufacturing Technology, Vol. 21, No. 8, pp. 579-585, 2003.
8. Huang, C. Z., Wang, J., Feng, Y. X. and Zhu, H. T., "Recent Development of Abrasive Water Jet Machining Technology," Key Engineering Materials, Vol. 315-316, pp. 396-400, 2006.
9. Zeng, J. Y. and Kim, T. J., "An Erosion Model of Polycrystalline Ceramics in Abrasive Waterjet Cutting," Wear, Vol. 193, Issue 2, pp. 207-217, 1996.
10. Finnie, I., "Some Reflections on the Past and Future of Erosion," Wear, Vol. 186-187, Issue 1, pp. 1-10, 1995.
11. Hutchings, I. M., "Ductile–Brittle Transition and Wear Maps for the Erosion and Abrasion of Brittle Materials," Journal of Physics D: Applied Physics, Vol. 25, Issue 1A, pp. A212-A221, 1992.
12. Ritter, J. E., Strzepa, P., Jakus, K., Rosenfeld, L. and Buckman, K. J., "Erosion Damage in Glass and Alumina," Journal of the American Ceramic Society, Vol. 67, No. 11, pp. 769-774, 1984.
13. Buijs, M., "Erosion of Glass as Modeled by Indentation Theory," Journal of the American Ceramic Society, Vol. 77, No. 6, pp. 1676-1678, 1994.
14. Wensink, H. and Elwenspoek, M. C., "A Closer Look at the Ductile–Brittle Transition in Solid Particle Erosion," Wear, Vol. 253, Issues 9-10, pp. 1035-1043, 2002.
15. Slikkerveer, P. J., Bouten, P. C. P., Veld, F. H. and Scholten, H., "Erosion and Damage by Sharp Particles," Wear, Vol. 217, Issue 2, pp. 237-250, 1998.

16. Hashish, M., "Pressure Effects in Abrasive-Waterjet (AWJ) Machining," Journal of Engineering Materials and Technology, Vol. 111, Issue 3, pp. 221-228, 1989.

17. Anstis, G. R., Chantikul, P., Lawn, B. R. and Marshall, D. B., "A Critical Evaluation of Indentation Techniques for Measuring Fracture Toughness: I, Direct Crack Measurements," Journal of the American Ceramic Society, Vol. 64, No. 9, pp. 533-538, 1981.

18. Marshall, D. B., Lawn, B. R. and Evans, A. G., "Elastic/Plastic Indentation Damage in Ceramics: The Lateral Crack System," Journal of the American Ceramic Society, Vol. 65, No. 11, pp. 561-566, 1982.

19. Lawn, B. R. and Evens, A. G., "A Model for Crack Initiation in Elastic/Plastic Indentation Fields," Journal of Materials Science, Vol. 12, No. 11, pp. 2195-2199, 1977.

20. Lawn, B. R., Evans, A. G. and Marshall, D. B., "Elastic/Plastic Indentation Damage in Ceramics: The Median/Radial Crack System," Journal of the American Ceramic Society, Vol. 63, No. 9-10, pp. 574-581, 1980.